JOURNAL OF CATALYSIS 142, 349–367 (1993)

On the Surface Acidity of Some Sulfate-Doped ZrO_2 Catalysts

C. MORTERRA, G. CERRATO, C. EMANUEL, AND V. BOLIS

Department of Inorganic, Physical, and Materials Chemistry, University of Turin, via P. Giuria 7, I-10125 Turin, Italy

Received November 10, 1992; revised February 26, 1993

XRD, HRTEM, and FTIR spectroscopy have been used to characterize the structure, morphology, and surface acidic activity of a family of sulfate-doped ZrO_2 systems, prepared by (low loading) sulfation with H_2SO_4 of ZrO_2 from Zr isopropoxide. Crystallinity and morphological features of the sulfated ZrO_2 systems are found to vary with preparative and activation conditions. Type and relative concentration of surface acidic sites (both Brønsted and Lewis centres) turn out to depend primarily on type and relative concentration of surface sulfates, which in turn depend on several preparative parameters. The role played by three of them is examined: the temperature of calcination of the nonsulfated ZrO_2 precursor, the overall surface concentration of sulfates, and the temperature of vacuum thermal activation of the sulfated ZrO_2 system. The ambient temperature adsorption of pyridine and of carbon monoxide, investigated by *in situ* FTIR spectroscopy, yield complementary information on the nature and heterogeneity of surface acidic centres.

1. INTRODUCTION

Sulfate-doped zirconia preparations (hereafter referred to as *s.d.-ZrO_2*) were found over a decade ago to possess, unlike other sulfated oxides, enhanced surface acidity and possibly superacid catalytic properties (e.g., see (*1, 2*)), and their surface and catalytic features have since attracted a great deal of interest (e.g., see (*3–9*)). Still, not all authors seem to agree on the superacid nature of these systems (e.g., see (*10*)), and the exact nature and origin of the strong acidity of s.d.-ZrO_2 remains controversial. In fact, some authors claim that protonic (Brønsted) acidity is always present and catalytically most important (*3, 7, 8*), whereas other authors report only the existence of a strong aprotic (Lewis) surface acidity (*5, 6*).

The aim of the present article is to contribute to the overall knowledge of these complex systems, and to show that, at least in the case of the particular family of s.d.-ZrO_2 catalysts dealt with here, both Brønsted and Lewis acidity can exist whenever some conditions are met. The relative amounts of the two types of acidic centres depend, grossly speaking, on the overall surface concentration of sulfate groups, as already suggested by other authors (*8*), but when observed in some detail they turn out to depend also on several other physical and/or chemical preparative parameters that seem to have escaped detection so far.

The precursors of the preparation and the preparation route of the s.d.-ZrO_2 catalysts, already indicated by others to be capable of producing some differences in surface chemical behaviour (*9*), are shown here to affect also the structural and/or morphological features of the materials.

2. EXPERIMENTAL

2.1. Materials

The s.d.-ZrO_2 catalysts dealt with here were prepared by adding at ambient temperature (by the method of "incipient wetness") dosed amounts of H_2SO_4 (0.1 *N*) to a pure ZrO_2 precursor, designated in the text and figures by the symbol *ZRP*. The physical and surface chemical characteristics of the latter material, prepared by the ambient temperature hydrolysis with H_2O of Zr isopropoxide (Zr-ip) as reported by Bensitel *et al.* (*6*), are well known and have been

0021-9517/93 $5.00

described in detail elsewhere (e.g., see (*6*, *11*) and references therein). The BET surface area of ZRP is $\approx$85 $m^2 g^{-1}$ after activation at $T \leq 523$ K, $\approx$55 $m^2 g^{-1}$ at 873 K, and $\approx$24 $m^2 g^{-1}$ at 1073 K.

The s.d.-ZrO_2 samples from (Zr-ip) are designated in the text and figures by the symbol $ZRS_{T_1}[n]T_2$, where:

(i) The subscript T_1 represents the temperature of pre-activation.

T_1 is the temperature (K) at which the pure ZrO_2 precursor was calcined in air for 4 hr (ZRP_{T_1}) before undergoing the ambient temperature sulfation process. The present contribution deals mainly with a homogeneous family of ZRS_{473} catalysts and, occasionally, with the catalysts ZRS_{873} and ZRS_{1073}, used for comparison.

The BET surface area of the ZRS_{473} catalysts varies (with sulfate loading) between 90 and 98 $m^2 g^{-1}$ with a slight increment of some 5–15% with respect to the starting ZRP_{473} material, whereas changes of surface area below $\approx$5% (and thus negligible) are observed for ZRS_{873} and ZRS_{1073} catalysts with respect to the relevant starting ZRP_{T_1} materials. A surface area that remains virtually unchanged upon sulfation represents a first distinctive difference between the ZrO_2/s.d.-ZrO_2 preparations from (Zr-ip), dealt with here, and those from $ZrOCl_2$ and $ZrO(NO_3)_2$, dealt with by other authors (*8*, *9*), in which the sulfation process produces an appreciable increase of surface area. A different texture of the starting oxides and, in particular, of the starting hydroxides ($T_1 \leq 573$ K) is thought to be responsible for the different behaviour.

(ii) The numeral [n] represents the nominal surface concentration of sulfates, expressed as S atoms per nm^2.

[n] corresponds for each sample to the maximum sulfate concentration, and was calculated assuming that all of the H_2SO_4 used for the sulfation process interacted with the surface of the material. The [n] figures, of which only a quasi-quantitative use will be made here, are bound to be somewhat imprecise, especially for high sulfate loadings, but no high sulfate loadings are considered in this note. Most of the authors who dealt with s.d.-ZrO_2 systems did not report the accuracy of their sulfate content figures (e.g., see (*8*, *9*)). Still, as pointed out by Bensitel *et al.* (*12*), analytical data relative to the actual surface concentration of sulfates cannot be very precise (consider, for instance, the uncertainty introduced by the determination of surface area, water content, etc.). Dealing with s.d.-ZrO_2 systems from (Zr-ip) similar to ours, Bensitel *et al.* (*12*) reported that, for S loadings up to $\approx$250 μmol g^{-1} (this corresponds in the concentration scale adopted here to [n] = 1.8–2 S atoms per nm^2, i.e., to the approximate completion of a first half monolayer), all of the SO_2 introduced becomes transformed into sulfates. For [n] > $\approx$2 S atoms per nm^{-2}, i.e., upon building up the second half monolayer of sulfates, increasing fractions of the added SO_2 do not remain at the surface of the system.

A few chemical analysis and FTIR experiments have been carried out on the sulfates of our s.d.-ZrO_2 samples from (Zr-ip), in order to check Bensitel's figures (*12*) and the ranges of validity of the nominal [n] figures adopted in this note as a reference concentration. The experiments seem to confirm that for [n] > 2–2.5 S atoms nm^{-2} either not all of the added H_2SO_4 reacts with the solid surface or some sulfate groups decompose, as the actual concentration of sulfates remaining on samples after activation at up to 673 K starts becoming increasingly lower than the maximum hypothetical [n] concentration. Two examples are reported, to show that in the range of low sulfate loadings considered here the [n] figures can be used as a reasonable reference concentration:

—In the case of preparation $ZRS_{473}[1.3]$, chemical analysis data led to a concentration of 1.38 SO_4 groups per nm^2 for the catalyst "as such" (in which all the H_2SO_4 added was obviously present in a form or the other), and of 1.34 SO_4 groups per nm^2 for the catalyst that was first heated at 673 K (to eliminate H_2SO_4 possibly unre-

acted). The difference (≈3.5%) is of the order of magnitude of the plain analytical error, and thus negligible, at least in comparison to other heavier sources of error. In the case of preparation $ZRS_{473}[2.6]$, the analytical data led to [*n*] figures (2.48 and 2.13 respectively) that differed by some 14%, in good agreement with the 12.5% deviation reported by Bensitel *et al.* (*12*) for nominal sulfur concentrations of 350 μmol g^{-1}. In the case of precrystallized s.d.-ZrO_2 systems, e.g., $ZRS_{873}[2.4]$, the difference in sulfate concentration between the plain material and that activated at 673 K was only some 8%.

—Figure 1 presents *in situ* FTIR spectra run in the spectral region of sulfates on the systems $ZRS_{473}[1.3]$ (upper spectra) and $ZRS_{473}[2.6]$ (lower spectra). The spectra were run on the catalysts in air (curves a), treated *in vacuo* at 300 K (curves b) and at 673 K (curves c), and then rehydrated at ambient temperature (curves d) and further activated at 300 K (curves e). It is seen that in the case of the lower S-loaded system (upper curves) some changes occur in the shape of the sulfate bands and in the structure of the sulfates, depending on the thermal treatment at 673 K and the degree of hydration of the system (as expected, and as discussed below in more detail), but no appreciable differences of either overall intensity or type of the bands are observed when the s.d.-ZrO_2 system is analyzed, in comparable conditions of hydration, before and after being treated *in vacuo* at 673 K. (Minor spectral differences are sometimes noted and are thought to be due to the thermal removal, at 673 K, of weak bands due to hydrocarbonaceous contaminants.) In the case of the higher loaded $ZRS_{473}[2.6]$ system (lower spectra), again no remarkable differences of band shape are observed in the samples, if the samples are analyzed under comparable conditions of hydration before and after the vacuum treatment at 673 K. Still, a net decrease (≈11%) of the integrated absorbance of the (almost unchanged) sulfate band envelope at 1420–860

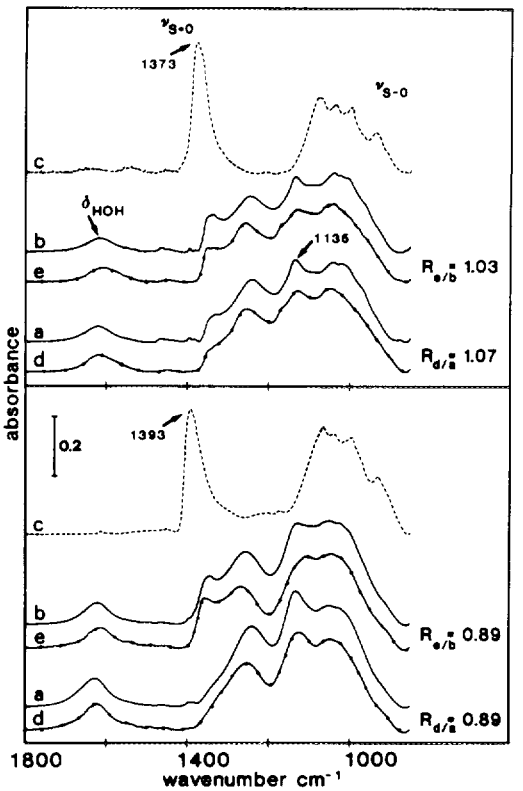

FIG. 1. Absorbance IR spectra in the 1800–850 cm^{-1} range (corresponding to the ν_{SO} modes of sulfates) of $ZRS_{473}[1.3]$ (upper section) and $ZRS_{473}[2.6]$ (lower section): (a) sample in air (200 Torr); (b) evacuated at ambient temperature; (c, broken line) activated at 673 K, (d, dotted line) the sample from c, after equilibration at ambient temperature in the vacuum system with ≈8 torr H_2O; (e, dotted line) after a further evacuation at ambient temperature. The quantities *R*, reported for the a–d and b–e spectral sets, represent the ratios of the integrated absorbances of the sulfate band envelopes (in the 1420–860 cm^{-1} interval) for sample d relative to a, and sample e relative to b.

cm^{-1} is noted, suggesting that a minor part of the added acid has been eliminated. In particular, a ν_{S-O} component centered at ≈1130 cm^{-1} seems to be preferentially reduced upon thermal treatment at 673 K.

(iii) The last figure in the samples symbol, the numeral T_2, represents the thermal activation stage reached by the catalyst. It is the temperature (K) at which the s.d.-ZrO_2 material was activated *in vacuo* for 1 hr be-

fore undergoing the IR/adsorption measurements.

2.2. Methods

All s.d.-ZrO_2 samples used for IR/adsorption measurements were in the form of thin powder layers ($\approx$8 mg cm^{-2}), deposited from isopropyl alcohol or water suspensions over a pure Si platelet. This procedure was necessary because the conventional self-supporting IR pellets are optically too thick to allow an adequate observation of the spectral region of surface sulfates.

IR/adsorption measurements were carried out *in situ* at a resolution of 2 cm^{-1}, using a Bruker 113v FTIR spectrometer equipped with MCT detector. Unsmoothed segments of the spectra of adsorbed probe molecules were occasionally band-resolved using an iterative program by Bruker (Simband), which sets only the number of spectral components and the desired accuracy, whereas all other spectral parameters (e.g., half-band width, percentage of Gaussian character, etc.) are allowed to float freely. All spectra of adsorbed CO were computer subtracted from the rovibrational contribution of the gaseous phase.

HRTEM data were obtained with a Jeol JEM 2000EX electron microscope, equipped with a top entry stage: the samples were dispersed in *n*-heptane, and then deposited on Cu grids coated with a holey carbon film.

XRD data were obtained with a Philips PW 1830 diffractometer ($K\alpha$ Co).

BET surface areas were determined with N_2 at 77 K with a Sorptomatic Ser. 1800 automatic apparatus (Carlo Erba, Milan).

3. RESULTS AND DISCUSSION

3.1. Structural and Morphological Data

Sample structure. Figure 2 shows segments of the XRD spectrograms of some ZRP_{T_1} samples and of some ZRS_{T_1} catalysts, loaded with comparable amounts of sulfates. It can be noted that:

(i) The starting precursor ZRP_{473} (Section a) is still amorphous, as is normally the case with all Zr hydrates calcined at $T \leq 683$ K, and exhibits two broad structureless XRD peaks, corresponding to the average interatomic distances of a disordered system. The broad peaks are located in the 2θ regions where discrete XRD peaks are present in crystalline ZrO_2 systems.

Surprisingly, the corresponding $ZRS_{473}[n]$ materials are crystalline (see Section b of Fig. 2, relating to $ZRS_{473}[1.3]$): the plain ambient temperature interaction with diluted

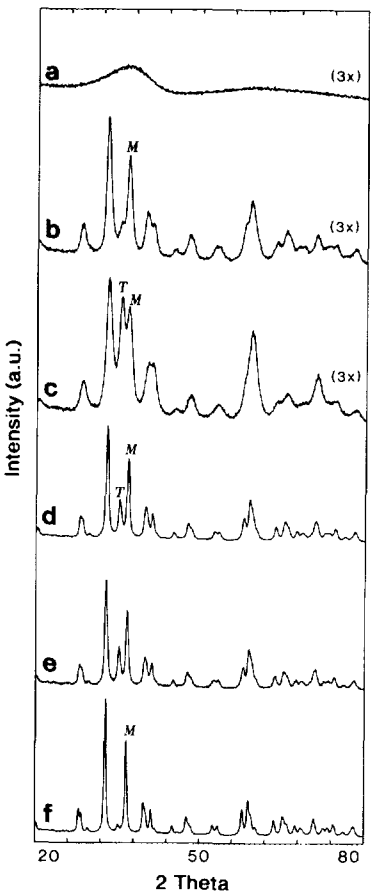

FIG. 2. Segments of the XRD patterns of some ZRP and related ZRS samples: (a) ZRP 473; (b) $ZRS_{473}[1.3]$ (c) ZRP 673; (d) ZRP 873; (e) $ZRS_{873}[1.2]$ (f): ZRP 1073. The letters M and T designate analytical peaks for the monoclinic and tetragonal ZrO_2 forms respectively. The XRD patterns in Sections a–c underwent a threefold *Y*-scale expansion.

H_2SO_4 brought about the crystallization of the amorphous Zr oxide/hydroxide system. The XRD peaks of $ZRS_{473}[1.3]$ are weak and quite broad, due to the still small crystal size, and correspond to a virtually pure monoclinic ZrO_2 form. Note that a thermal crystallization of the amorphous ZRP system, yielding XRD peaks with intensity and breadth comparable to those of Fig. 2b, is obtained on firing at 673–723 K (see, for instance, Section c of Fig. 2, relating to ZRP 673), but in that case the resulting crystalline ZrO_2 system is an ≈70–30% mixture of the monoclinic and tetragonal forms.

This is a second distinctive difference between the ZrO_2/s.d.-ZrO_2 preparations from (Zr-ip), dealt with here, and those from $ZrOCl_2$ and $ZrO(NO_3)_2$, dealt with by other authors (*8, 9*), in which the sulfation process first delays the crystallization (up to ≈750 K) and then, at higher temperatures, leads almost exclusively to the tetragonal ZrO_2 form.

(ii) The precursor materials ZRP 873 (Fig. 2d) and ZRP 1073 (Fig. 2f) are crystalline ZrO_2: the XRD peaks are much sharper, due to the increased crystal size, and the crystalline form is mainly monoclinic with a minor amount of tetragonal form which decreases fast with preactivation temperature. The corresponding catalysts $ZRS_{873}[1.2]$ (Fig. 2e) and $ZRS_{1073}[1.0]$ (not shown) are also crystalline, and the XRD peak widths and the relative amounts of tetragonal vs monoclinic form remain much as they were in the sulfate-free precursors. This means that, unlike the case of amorphous ZrO_2 preparations, sulfation with diluted H_2SO_4 of microcrystalline ZrO_2 does not appreciably alter the bulk structure of the starting material. This datum is consistent with the virtual constancy of BET surface area through the sulfation process.

Sample Morphology. Figure 3 reports some details of the HRTEM micrographs of the ZRP and ZRS samples shown in Fig. 2. It can be noted that:

(i) The starting ZRP 473 preparation (Section a) is confirmed to be virtually amorphous. Still, here and there the compact and shapeless mass shows small patches of irregularly shaped interference fringes, typical of crystalline systems. The fringes could be due to small microcrystalline islands produced by prolonged exposure to the high energy electron beam. Considering that amorphisation of crystalline materials upon exposure to the electron beam in the electron microscope is a phenomenon certainly more frequent than the opposite one, this might mean that the texture of the Zr oxide/hydrate from (Zr-ip) is that of a metastable quasi-crystalline system, as also suggested by the fast crystallization brought about by the sulfation process, and revealed also by XRD data (see Fig. 2b).

Consistently, the HRTEM micrograph of the corresponding $ZRS_{473}[1.3]$ catalyst (shown in Fig. 3b) confirms that, after sulfation, crystalline particles of 8–12 nm side have been produced, in agreement with what is observed in Fig. 2b. The particles, still disorderly distributed and very closely packed, present discrete patches of rather regular interference fringes (monitoring that the "top" termination of the particles is mainly along some regular low-index crystal planes), and are delimited by contours shaped most irregularly (revealing that the "side" termination of the newly formed crystallites is, in crystallographic terms, highly defective; see, for instance, the irregularly stepped particle terminations indicated by the arrows in Fig. 3b).

Section c of Fig. 3, relating to ZRP 673, shows that particle size and morphology fairly similar to those of $ZRS_{473}[n]$ are obtained, upon thermal treatment of the pure ZrO_2 ZRP system, only at 673–723 K, confirming the XRD datum of Fig. 2c, and the indication that the sulfation process accelerates the crystallization of ZrO_2 from (Zr-ip).

(ii) The reference ZRP 873 system (shown in Fig. 3d, and described in more detail elsewhere (*11*)) is made up of well separated individual coin-shaped particles of some 12–18 nm diameter. The most frequent interference fringe patterns exhibit a regular

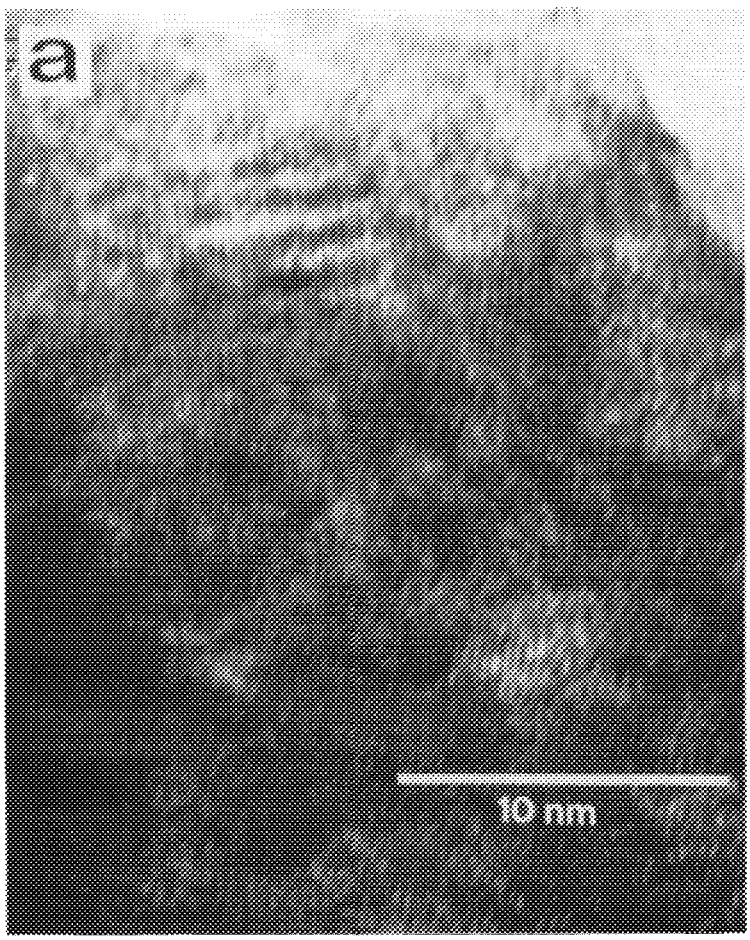

FIG. 3. HRTEM images of some ZRP and related ZRS samples (a) ZRP 473; (b) $ZRS_{473}[1.3]$; (c) ZRP 673; (d) ZRP 873; (e) $ZRS_{873}[1.2]$; (f) ZRP 1073.

spacing of ≈0.3 nm and indicate that a "top" termination of the particles along the (111) crystal plane of monoclinic ZrO_2 is predominant. Other low-index crystal planes, e.g., the (001) plane with a fringe spacing of ≈0.50 nm, are met with a much lower frequency. Most of the large steps observed in Fig. 3b have now disappeared, but the roundish contours of the coin-shaped particles indicate a still fairly abundant amount of crystallographically defective "side" terminations.

The corresponding $ZRS_{873}[1.2]$ system (see Fig. 3e) presents particle size and morphology very similar to those of the parent ZRP preparation. Minor differences consist in the fact that the ZRS particles are often larger (≈20 nm), definitely less separated from one another, and more frequently present sharp edges (see, for instance, the arrows in Fig. 3e) that suggest for the sulfated system a somewhat decreased number of defective terminations. The morphology of $ZRS_{873}[n]$, only marginally modified with respect to the parent ZRP 873, is consistent with the constant BET and XRD data reported in previous sections.

(iii) The ZRP 1073 system (Fig. 3f), which is now pure monoclinic ZrO_2, and the corresponding $ZRS_{1073}[0.1]$ system (not shown in the figure) present virtually identi-

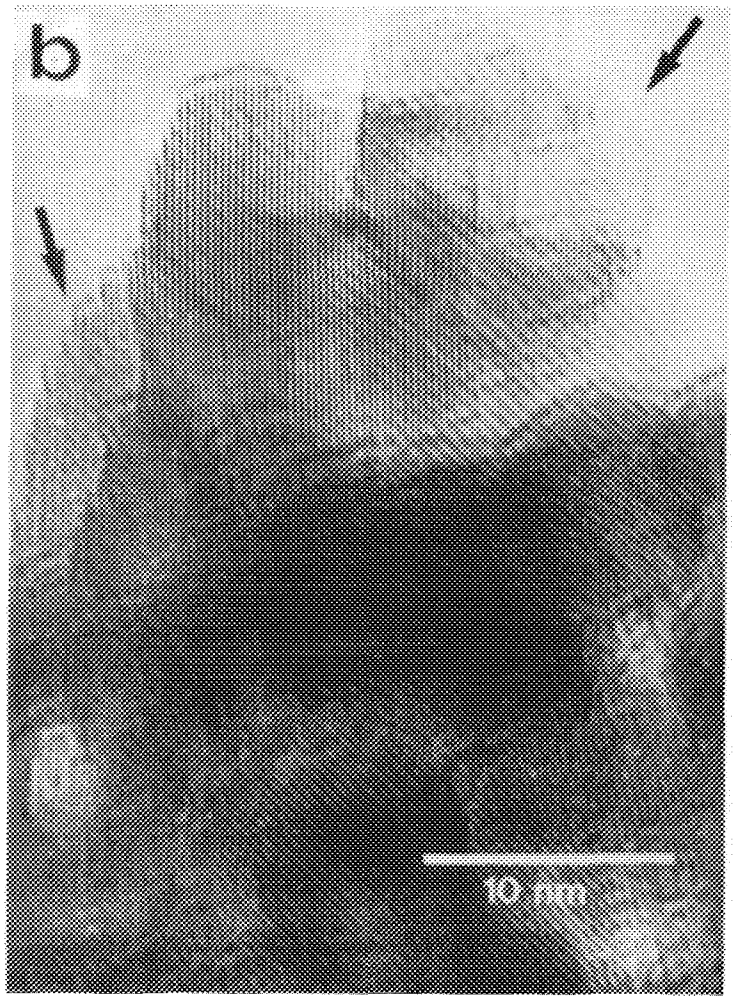

FIG. 3—*Continued*

cal morphology and particle size. Due to the incipient sintering process, the particles are definitely larger (side: 25–35 nm), and their crystalline order is much higher: in fact they exhibit extended patches of fairly regular interference fringes, still most frequently corresponding to the (111) crystal plane of monoclinic ZrO_2, and are delimited by long regular edges which form either sharp or only slightly roundish intersections with one another. This suggests that most of the crystallographically defective configurations have been eliminated. Again, size and morphology of the particles, which remain virtually unchanged through the sulfation process, are consistent with virtually unchanged BET and XRD data.

3.2. The Surface Sulfates

Sulfate groups that form at the surface of most oxidic systems possess, in general, similar structures, and the literature dealing with the spectral features of surface sulfated oxides is quite vast. In the particular case of s.d.-ZrO_2 systems, the characterization and assignment of surface sulfates proposed by Bensitel *et al.* (*12*) is most detailed and convincing, so that reference will be made

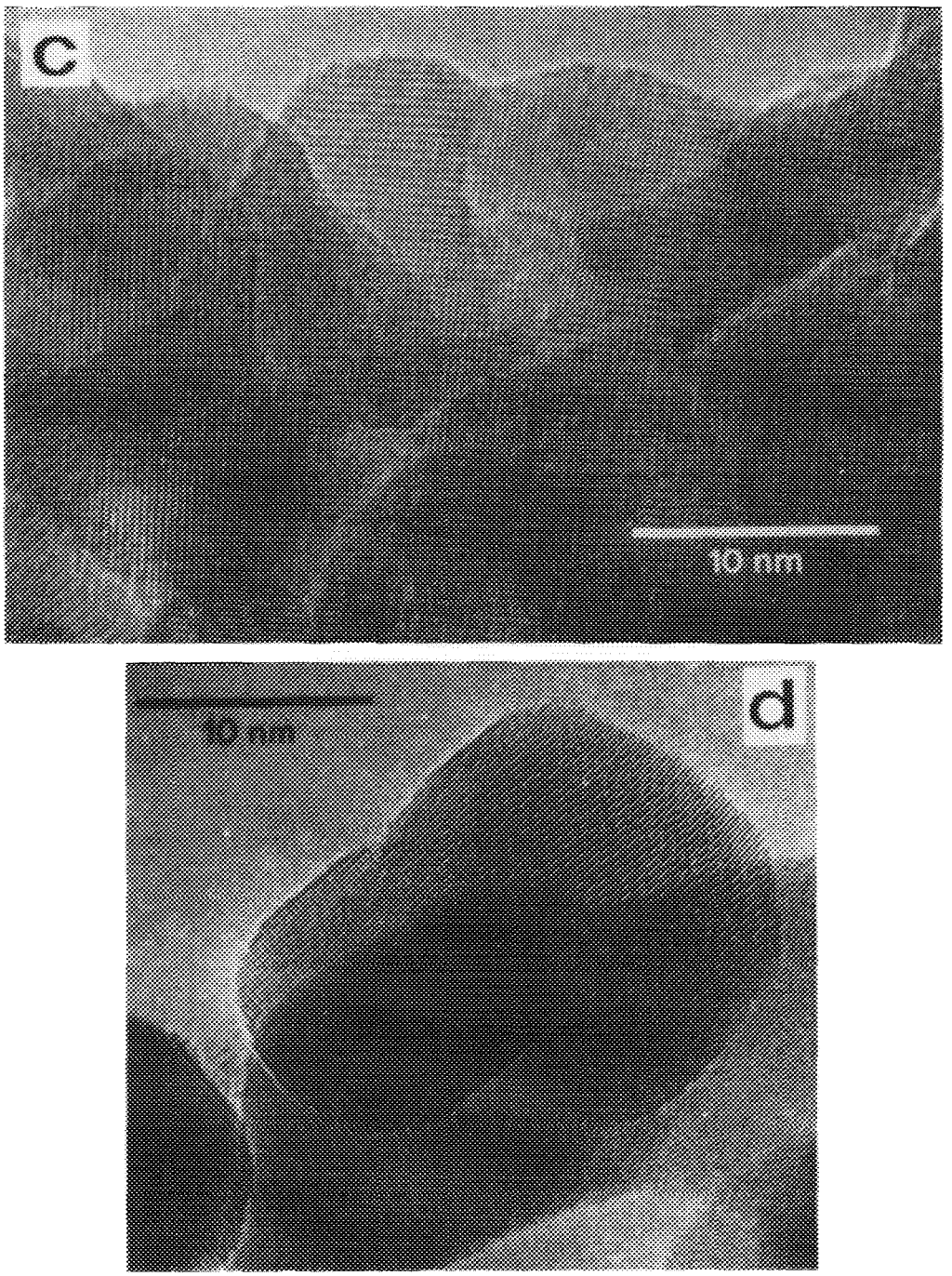

FIG. 3—*Continued*

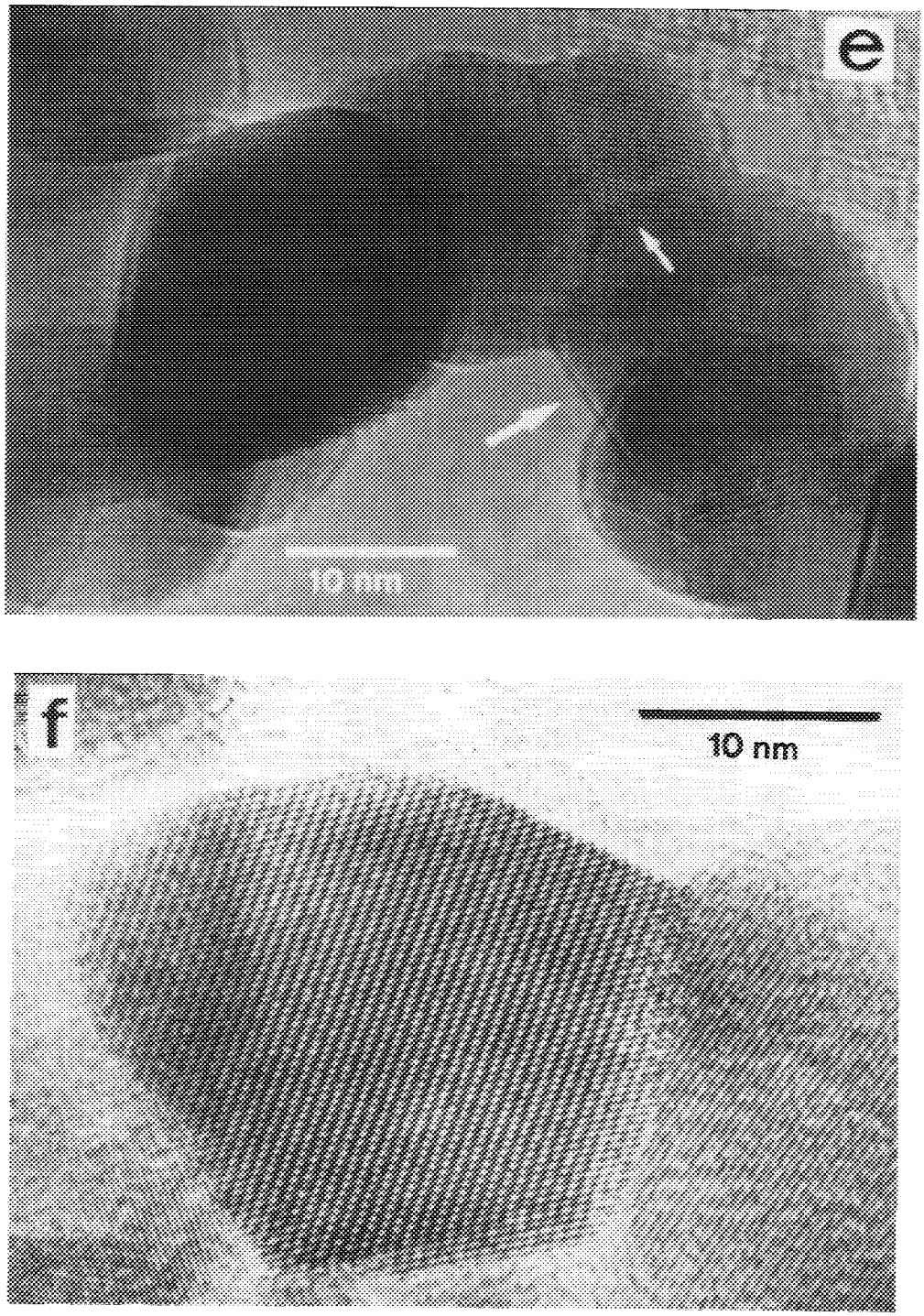

FIG. 3—*Continued*

mainly to their findings without entering too much into details.

It is recalled that, on most oxides that are fully hydrated (e.g., in air) or only slightly dehydrated, surface sulfates are in a highly ionic form and present several ν_{SO} bands, mainly localized at $\tilde{\nu} \leq \approx 1250$ cm^{-1}, reminiscent of the sulfate bands observed on hydrated crystalline inorganic sulfates and/or on sulfato complexes (*13*) (see, for instance, curves a–b and d–e in Fig. 1, relating to $ZRS_{473}[1.3]$). In contrast, sulfates at the surfaces of oxides brought *in vacuo* to medium-high dehydration stages possess a highly covalent character. In fact they present high frequency $\nu_{S=O}$ stretching bands (located at $\tilde{\nu} \geq 1350$ cm^{-1}, and similar to the $\nu_{S=O}$ modes of organic sulfonyl-containing compounds (*14*)), besides a certain number of lower frequency bands ($\tilde{\nu} \leq 1150$ cm^{-1}) due to ν_{S-O} stretching modes (see, for instance, curves c in Fig. 1).

In the specific case of the s.d.-ZrO_2 systems activated at $T \geq 650$ K, there are several families of covalent surface sulfates, and consequently the spectral pattern in the 1450–800 cm^{-1} range is quite complex. Most of the sulfates of s.d.-ZrO_2 have been conclusively shown by Bensitel *et al.* (*12*) not to carry  groups, but to possess single (i.e., isolated and vibrationally uncoupled) S=O oscillators, and have been postulated to be bonded to the oxide network by more than two S–O–Zr bridges.

Up to a certain sulfate loading, indicated by Bensitel *et al.* as ≈250 μmol g^{-1} (*12*) (in the concentration units adopted here, it roughly corresponds to $[n] = \approx 1.8$ nm^{-2}), the sulfates at the surface of s.d.-ZrO_2 are thought to be mainly in the form of isolated $[SO_4]^{2-}$ groups ($\nu_{S=O} \leq 1400$ cm^{-1}). The sulfates start to become polynuclear complex sulfates (possibly of the $[S_2O_7]^{2-}$ type) characterized by $\nu_{S=O} \geq 1400$ cm^{-1} (*11*) when the sulfate loading is higher, though still quite far from reaching the full monolayer (the average value for a monolayer of $[SO_4]^{2-}$ groups corresponds to $[n] \approx 4$ nm^{-2} (*8*)).

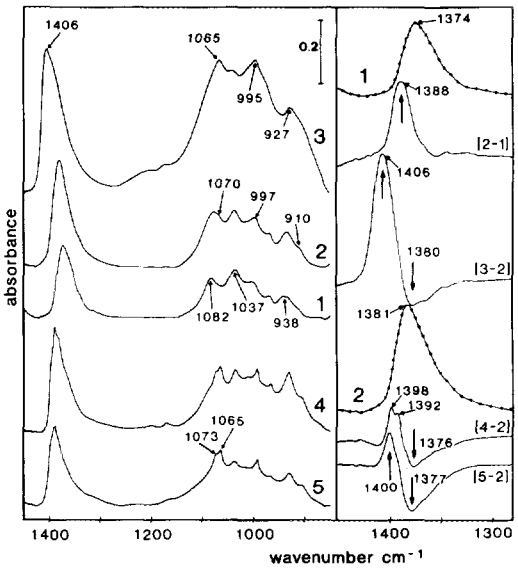

FIG. 4. Absorbance IR spectra of some ZRS samples in the whole S/O stretching region (left-hand section) and in the S=O stretching region (right-hand section, *X*-scale expanded): (1) $ZRS_{473}[0.65]673$; (2) $ZRS_{473}[1.3]673$; (3) $ZRS_{473}[2.6]673$; (4) $ZRS_{873}[1.2]673$; (5) $ZRS_{1073}[1.0]673$. In the differential spectra (right-hand section, solid-line curves) the vertical arrows pointing up indicate the $\nu_{S=O}$ components whose relative amounts increased, and the arrows pointing down the components whose relative amounts decreased.

Curves 1–3 of Fig. 4 report the spectral pattern of surface sulfates formed on some ZRS_{473} samples characterized by increasing sulfate loadings and vacuum activated at 673 K. The spectra exhibit several differences, among which the following are thought to be important:

(i) The system of isolated sulfates, which is confirmed to dominate for S loadings below ≈1.5 atoms per nm^2 (see curves 1, 2 of Fig. 4), is quite complex and both $\nu_{S=O}$ and ν_{S-O} bands are made up of several slightly different and poorly resolved components. Moreover, the building up of the first half monolayer of sulfates is gradual: sulfates characterized by the $\nu_{S=O}$ band at the lowest frequencies ($\nu_{S=O}$ = 1360–1375 cm^{-1}; broadish and asymmetrical on the low $\tilde{\nu}$ side) and by ν_{S-O} modes at ≈1085, ≈1035, and ≈940 cm^{-1} are formed first, and are almost

the only species formed at the surface of low S-loaded ZRS_{473} catalysts (see curve 1 of Fig. 4). Isolated sulfates characterized by a $\nu_{S=O}$ mode in the 1380–1390 cm^{-1} range (see curve 2 and the scale-expanded [2-1] differential on the right-hand side of Fig. 4) and by ν_{S-O} modes at ≈1070, ≈995, and ≈910 cm^{-1} respectively (evidenced by differential spectra, not shown in the figure) start forming for concentrations above ≈0.8 S atoms per nm^2, and prevail at the surface of medium S-loaded ZRS_{473} catalysts.

(ii) On passing from (nominal) S concentrations of ≈1.3 S atoms per nm^2 to ≈2.6 atoms per nm^2 (i.e., after completion of the first half monolayer of sulfates; see curves 2 and 3 of Fig. 4), complex spectral changes occur, best monitored in the $\nu_{S=O}$ range by the differential spectrum [3-2] reported on the right-hand section of Fig. 4): the highest $\nu_{S=O}$ mode moves to ≈1405 cm^{-1}, while part of the $\nu_{S=O}$ band at ≈1385 cm^{-1} declines, and in the ν_{S-O} region new strong and broader components form at ≈1065, ≈995, and ≈925 cm^{-1}. These changes are thought to correspond to passage from a regime of isolated sulfates to one in which complex polynuclear sulfates are also present, as expected on the basis of the assignment proposed by Bensitel *et al.* (*12*).

Curves 4 and 5 of Fig. 4 show, for comparison purposes, the spectra of sulfates formed at the surfaces of ZRS_{873}[1.2]673 and ZRS_{1073}[1.0]673 respectively, i.e., on ZrO_2 systems carrying a nominal sulfate concentration similar to that of the ZRS_{473} sample of curve 2, but progressively better crystallized. It can be noted that, consistent with what is observed in the case of ZRS_{473}[1.3], mainly isolated sulfate groups (characterized by $\nu_{S=O} < 1400\ cm^{-1}$) also form at the surface of these medium S-loaded specimens, but the isolated sulfates characterized by the lowest $\nu_{S=O}$ frequencies, and which form first on ZRS_{473}, become progressively missing. This is better shown by the surface-area normalized differential spectra [4-2] and [5-2] on the right-hand section of Fig. 4: as the preactivation temperature of the ZrO_2 precursor increases, the relative concentration of sulfates with $\nu_{S=O} \geq 1380\ cm^{-1}$ progressively increases (see the arrows pointing up), whereas that of sulfates with $\nu_{S=O} \leq 1375\ cm^{-1}$ declines (see the arrows pointing down).

With the aid of the structural/morphological data reported in the previous section, the following conclusion can be drawn: the isolated sulfates characterized by the lowest $\nu_{S=O}$ modes ($\nu_{S=O} \leq 1375\ cm^{-1}$) are mainly ascribable to sulfate groups formed in more energetic configurations (in fact, when they do form, they form first) and corresponding to crystallographic defects (i.e., steps, corners, and high-index planes, which gradually anneal with thermal sintering), whereas the isolated sulfates whose $\nu_{S=O}$ mode lies in the 1400–1380 cm^{-1} range are mainly formed on the less energetic regular patches of low-index crystal planes (which with thermal sintering gradually become the predominant termination of the ZrO_2 crystallites).

Note that, on better and better crystallized systems, the $\nu_{S=O}$ band and the ν_{S-O} bands of the latter species tend to be resolved into several slightly different discrete components, suggesting that several crystal planes, energetically slightly different from one another, are most likely exposed.

Note also that the correlations here proposed between type of sulfates and crystals morphology apply only to the family of s.d.-ZrO_2 systems from (Zr-ip). In fact at the moment no data of this type are available on the particles' morphology nor on the spectra of sulfates formed on s.d.-ZrO_2 systems from $ZrOCl_2$ and/or $ZrO(NO_3)_2$, and the crystallographic behaviour of the latter systems upon sulfation is quite different.

3.3. The Adsorption of Pyridine: Brønsted and Lewis Acidity

It is well known that the IR spectrum of adsorbed pyridine (py) is one of the most suitable analytical tools to distinguish, at the surface of oxidic systems, Brønsted protonic acidity and σ-coordinative Lewis acidity (e.g., see (*15, 16*) and references therein). Therefore, the controversial nature of the

surface acidity of some of the ZRS systems dealt with in the previous sections has been tested by *in situ* FTIR spectroscopy of the ambient temperature adsorption of py.

Medium temperature activated samples. The solid-line curves in Fig. 5 show segments of the IR spectra (in the 1650–1500 cm^{-1} range, i.e., in the analytical range of the 8a–8b and of some of the 19a–19b "ring" modes of py) relating to the adsorption of py at the surface of some ZRS systems activated at 673 K. With the aid of the schematic spectral pattern reported in the top section of Fig. 5, it can be noted that:

(i) On ZRS_{473}[0.65]673 (curve 1, solid line) there is no formation of Brønsted coordinated py, but only the formation of abundant Lewis coordinated py (marked [py-L] in curve 1). The 8a py band of [py-L] adsorbed on this s.d.-ZrO_2 system is single and is centered at $\approx$1605 cm^{-1}, i.e., some 3 cm^{-1} higher than in the case of [py-L] adsorbed on the corresponding ZRP system (*6*): this indicates that the presence of the surface sulfate species, most likely isolated sulfate groups localized in crystallographically defective configurations, increased very slightly by inductive effects the acidity of (all of) the Lewis acidic centres present in the system.

(ii) Also on ZRS_{473}[1.3]673 (curve 2, solid line) the amount of Lewis coordinated py is large, whereas the amount of Brønsted coordinated py (marked [py-B] in curve 2) is not zero, but fairly small. Also on ZRS_{473}[1.3]673 the 8a py band of [py-L] is single and is now centered at $\approx$1608 cm^{-1}, meaning that the increased overall amount of sulfates and the varied type of sulfates have further increased the acidity of (all of) the Lewis acidic centres still present at the surface.

(iii) On ZRS_{473}[2.6]673 (curve 3, solid line) the amount of Brønsted coordinated py has increased appreciably, although it still represents a minor fraction of the overall py adlayer. The 8a py band of [py-L] is still single, and is now centered at $\approx$1612 cm^{-1}, i.e., some 10 cm^{-1} higher than on the sulfate-free system, indicating that the further increased overall concentration of sulfates and the incipient formation of complex sul-

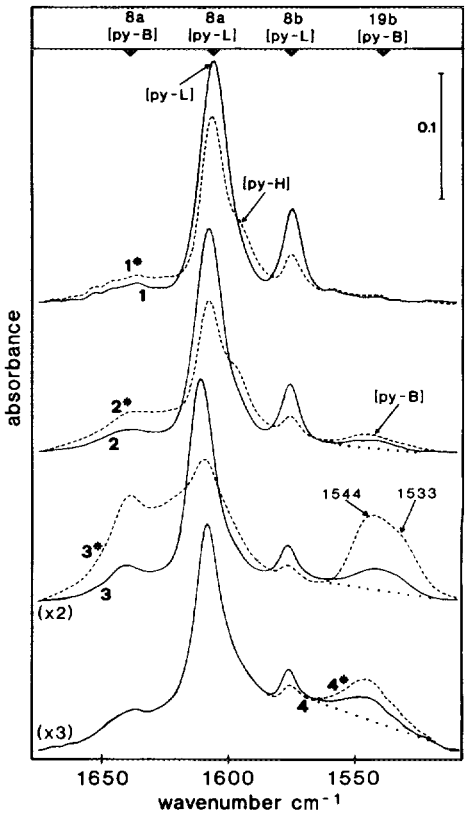

FIG. 5. Segments of the absorbance IR spectra of pyridine (py) adsorbed at 300 K on some ZRS samples. Solid-line spectra: 10 torr py were adsorbed, and the excess py was pumped off, on ZRS_{473}[0.65]673 (1), ZRS_{473}[1.3]673 (2), ZRS_{473}[2.6]673 (3), and ZRS_{873}[1.2]673 (4). (Spectra 3 and 4 were *Y*-scale expanded relative to spectra 1 and 2 by the factors shown on the curves, to compensate for the lower py activity caused by the increased sulfates concentration (3) and the decreased surface area (4)). Broken-line spectra (curves marked with asterisks): On the samples of curves 1–4 (solid-line spectra) 2 Torr water was dosed at 300 K, and the excess water was pumped off at the same temperature. (Spectra 3* and 4* were *Y*-scale expanded by the same factors as the corresponding spectra 3 and 4). Symbols and arrows in the top section of the figure indicate the average spectral positions of some of the analytical "ring" stretching modes of Brønsted and Lewis bound py. Brønsted and Lewis bound py are represented by the symbols [py-B] and [py-L], respectively; the symbol [py-H] represents py H-bonded to surface OH groups.

fates brought about a strong increase of acidity of (all of) the Lewis acidic centres still present at the surface. Considering that for nominal sulfate concentrations [n] > ≈2 S atoms per nm^{-2} not all of the sulfate groups added actually remain in the system as surface sulfates, it is deduced that complex polynuclear sulfates, most likely localized on regular crystal planes, have a stronger (inductive) effect of acidity enhancement on the surface Lewis acidic sites than the other types of surface sulfates.

(iv) On the reference ZRS_{873}[1.2]673 catalyst (curve 4, solid line), the amount of Brønsted coordinated py is also small, but relative to the Lewis coordinated species, whose 8a mode is centered at ≈1608 cm^{-1}, the amount is much higher than in the case of the ZRS_{473} sample of curve 2, although the overall surface sulfate concentration on the two specimens is virtually the same (the gross (integral) intensity ratio between the 8b mode of [py-L] and the 19b mode of [py-B] is ≈2.5 and ≈0.4 for ZRS_{473}[1.3]673 and ZRS_{873}[1.2]673, respectively).

A first important conclusion can thus be drawn from these data: besides the abundant σ-coordinative Lewis acidity, whose strength is enhanced by the presence of surface sulfates, some protonic Brønsted acidity can also be present at the surface of s.d.-ZrO_2 catalysts from (Zr-ip), activated at medium temperatures. The amount of Brønsted acidic sites tends to increase with increasing overall sulfate loading, as recently indicated by Nascimento *et al.* (*8*), but the formation of Brønsted acidic centres is not merely a matter of sulfate concentration. In particular, no appreciable Brønsted acidity is produced when isolated sulfates are formed only on crystallographically defective configurations, whereas some Brønsted acidity is produced when isolated sulfates and, above all, complex sulfates also start being formed on regular low-index ZrO_2 crystal planes.

The solid-line spectra of curves 2–4 of Fig. 5 indicate that, in any case, Brønsted acidity is in comparison with Lewis acidity only a minor component of the overall surface acidity of ZRS systems characterized by medium-high S-loadings, when activated at medium temperatures. This may explain in part why other authors reported that, in the case of some medium-high S-loaded s.d.-ZrO_2 systems from (Zr-ip) activated at relatively high temperatures, no Brønsted activity could be noted (*6*).

Highly hydrated samples. As a further step, we have checked if the Brønsted/Lewis acidity ratio depends on other parameters, besides the sulfate loading, and in particular on the surface hydration degree. The broken-line curves reported in Fig. 5, and designated by numerals marked with an asterisk, show the spectral changes produced in the corresponding solid-line spectra of preadsorbed py by the ambient temperature adsorption of small doses of water vapour. It can be noted that:

(i) When no Brønsted acidity is detectable at the surface of a ZRS catalyst activated at 673 K (curve 1), in that the catalyst contains only isolated sulfates located on crystallographically defective sites ($\nu_{S=O} \leq 1375$ cm^{-1}), surface rehydration does not produce any protonic acidity (see curve 1*). In fact, upon hydration, there is only the desorption of some of the Lewis coordinated species (see, for instance, the decrease of the 8b mode) and the conversion of part of the Lewis coordinated py species into H-bonded ones ([py-H]), due to the partial rehydroxylation of the catalyst surface. The acidic strength of the residual [py-L] species is not modified by the rehydration process, as the spectral position of the 8a py mode remains unchanged.

(ii) When, on materials with higher S loadings, isolated and/or complex sulfates are also present on regular patches of low-index crystal planes ($\nu_{S=O} \geq 1380$ cm^{-1}), surface rehydration converts some of the abundant Lewis-bound py species (σ-coordinated to coordinatively unsaturated Zr^{4+} sites that were produced upon vacuum surface dehydration) into Brønsted py species (compare, for instance, curves 2–4 with curves 2*–4*).

Not all of the Lewis centres are converted into Brønsted ones upon rehydration, and the fraction of Lewis-bound py that can be converted into Brønsted-bound py is higher the higher the sulfates concentration (in fact on $ZRS_{473}[2.6]673$ [py-B] becomes, after rehydration, the predominant component of the surface py adlayer). This suggests that complex sulfates, which form most favourably at high S-loadings on regular crystal planes, are favoured centres for the production of protonic Brønsted acidic sites.

A second important conclusion can be now drawn from these data: for any s.d.-ZrO_2 catalyst from (Zr-ip) carrying sulfates in "regular" crystallographic configurations, the Brønsted/Lewis acidity ratio (as given by the intensity ratio of analytical bands specific to the [py-B] and [py-L] species) is not an absolute parameter, but depends on the surface dehydration/rehydration degree of the catalyst. Therefore, Brønsted/Lewis acidity ratio plots of the type recently proposed by Nascimento *et al.* (*8*) for the characterization of s.d.-ZrO_2 catalysts from $ZrOCl_2$ probably have only a relative meaning, and ought to be used with caution.

As for the Brønsted-bound py species, note that the analytical 19b py band is broad and most likely double (e.g., see curve 3* of Fig. 5, with components at $\approx$1545 and $\approx$1535 cm^{-1}, and curve 1* in Fig. 6a reported below); the heterogenous nature of the protonic surface acidic sites formed on s.d.-ZrO_2 systems from (Zr-ip) is thus revealed, heterogeneity that could not be revealed by py adsorption when the sites were in the (aprotic) Lewis acid configuration.

High temperature activated samples. Curves 2–4 of Fig. 5 showed that samples with medium-high S loadings and activated at medium temperatures possess both Brønsted (few) and Lewis sites; a similar situation has been met also by other authors with other s.d.-ZrO_2 systems (e.g., see (*8*, *9*)).

We have finally checked if all of the Brønsted acidic centres, induced by surface sulfates characterized by $\nu_{S=O}$ modes at $\tilde{\nu} \geq 1380$ cm^{-1}, can be reversibly converted into Lewis acidic centres upon surface dehydroxylation at higher temperatures. To do so, the sulfate-rich $ZRS_{473}[2.6]673$ system dealt with in curves 3 and 3* of Fig. 5 was stepwise vacuum activated at $T > 673$, and after each activation treatment py was adsorbed at ambient temperature and, on preadsorbed py, small amounts of water were dosed.

The spectral data relative to the py/water uptake on the $ZRS_{473}[2.6]T_2$ systems and to the relevant surface sulfates are shown in Fig. 6, sections a and b respectively. It has been observed that:

(i) For activation temperatures up to $\approx$750 K, all spectral changes induced in the sulfate bands by the vacuum thermal treatments (e.g., see curve 1 of Fig. 6b), by a subsequent py adsorption (curve 1'b), and by rehydration after py uptake (curve 1*b) turn out to be reversible. But when the vacuum activation is carried out at higher temperatures, surface sulfates start decomposing, and irreversible changes are produced in the relevant spectra as well as in the activity towards py.

(ii) Activation at 773 K (see curve 2 of Fig. 6b, and the [2-1] differential therein) brings about a first partial sulfate decomposition, with conversion of part of the complex sulfates (formed mainly on regular crystal planes, and characterized by $\nu_{S=O} \geq 1400$ cm^{-1}) into isolated sulfates ($\nu_{S=O}$ in the 1400-1380 cm^{-1} range). This is best shown by the [2-1] differential, where the arrow pointing down indicates the species that were eliminated by the thermal treatment ($\nu_{S=O} \geq 1400$ cm^{-1}), and the arrow pointing up shows the species that were formed ($\nu_{S=O} \approx 1380$ cm^{-1}). Note that no changes are produced in the spectral region typical of the sulfates localized on crystallographically defective centres ($\nu_{S=O} \leq 1375$ cm^{-1}).

Py/water uptake on $ZRS_{473}[2.6]773$ shows that the thermal treatment eliminated $\approx$50% of the Brønsted centres (compare the 19b band of [py-B] at $\approx$1540 cm^{-1} in curves 1*

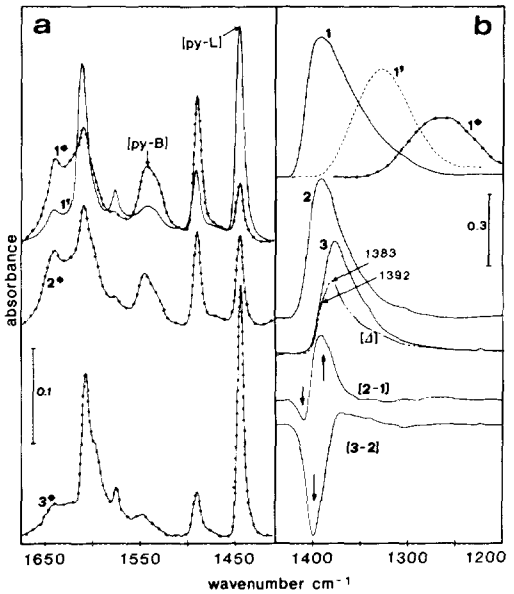

FIG. 6. Effect of the vacuum activation temperature of a $ZRS_{473}[2.6]$ catalyst on the spectrum of py adsorbable at 300 K (a) and the spectrum of surface sulfates (b). (1) $ZRS_{473}[2.6]673$; (1') 10 Torr py was adsorbed on 1, and the excess py evacuated at 300 K; (1*) 2 Torr H_2O was adsorbed on 1', and the excess H_2O evacuated at 300 K. (2) $ZRS_{473}[2.6]773$; (2*) 10 Torr py was adsorbed on 2, and the excess py evacuated at 300 K; then, 2 Torr H_2O was adsorbed, and the excess H_2O evacuated at 300 K. (3) $ZRS_{473}[2.6]823$; (3*) 10 Torr py was adsorbed on 3, and the excess py evacuated at 300 K; then, 2 Torr H_2O was adsorbed, and the excess H_2O evacuated at 300 K. Differential spectra (in the $\nu_{S=O}$ region): $[\Delta] = ZRS_{473}[2.6]823 - ZRS_{473}[0.65]823$; $[2-1] = ZRS_{473}[2.6]773 - ZRS_{473}[0.65]673$; $[3-2] = ZRS_{473}[2.6]823 - ZRS_{473}[0.65]773$. In the differential spectra the vertical arrows pointing up indicate the $\nu_{S=O}$ components whose relative amount increased, and the arrows pointing down the components whose relative amount decreased.

and 2* of Fig. 6a), while the amount of Lewis centres, no longer convertible into Brønsted ones upon rehydration, has increased (compare the 19b band of [py-L] at ≈ 1445 cm^{-1} in curves 1* and 2* of Fig. 6a).

(iii) Activation of 823–873 K (see curve 3 of Fig. 6b, and the [3–2] and [Δ] differentials therein) eliminates completely the complex sulfates (in fact no absorption remains at $\tilde{\nu} \geq 1400$ cm^{-1}), and a small fraction of the isolated sulfates ascribed to the regular patches of low-index crystal planes. In fact the [Δ] differential ($[\Delta] = ZRS_{473}[2.6]823 - ZRS_{473}[0.65]823$) shows that after the treatment at 823 K a fair amount of isolated sulfates still remains on the faces (see the poorly resolved $\nu_{S=O}$ components at ≈ 1383 and ≈ 1392 cm^{-1}), whereas virtually no changes are yet produced in the sulfates on defects ($\nu_{S=O}$ mode at $\nu \leq 1375$ cm^{-1}), which are the only species formed on low-loading ZRS_{473} samples.

A subsequent py/water uptake (see curve 3* of Fig. 6a) shows that the treatment at 823 K eliminated (almost) all of the residual Brønsted acidic activity, and increased further the amount of Lewis centres not convertible into Brønsted ones upon rehydration. It is so deduced that mainly responsible for the protonic Brønsted acidity of s.d.-ZrO_2 systems are:

—all the complex polynuclear sulfates;

—only the highest $\nu_{S=O}$ component(s) of the isolated sulfates located on some low-index crystal planes.

A third important conclusion concerning the Brønsted/Lewis acidity controversy can be now drawn: for any s.d.-ZrO_2 catalyst from (Zr-ip), the Brønsted/Lewis acidity ratio depends, besides the parameters already mentioned above, also on the highest activation temperature reached by the sulfated system, as the sulfates responsible for the protonic acidity are thermally the most labile fraction of the surface sulfate layer. Also this datum may explain in part why, in the case of some high S-loaded s.d.-ZrO_2 materials, coming from (Zr-ip) as ours and dealt with by other authors, no Brønsted activity at all could be observed (*6*): if vacuum activation temperatures above ≈ 773 K were reached by the catalyst in any stage of the treatments, the sulfates of the proper type were no longer present at the surface.

3.4. The Adsorption of Carbon Monoxide: Lewis Acidity

The adsorption of py, dealt with in the previous section, revealed the double nature

of the surface acidity of s.d.-ZrO_2 catalysts from (Zr-ip), i.e., the presence of both Brønsted and Lewis acidity, as well as a probable heterogeneity of the Brønsted acidic sites. But it was unable to show if the Lewis surface acidic sites, though in part related to the Brønsted ones, are homogeneous or heterogeneous in nature. In this respect it is recalled that the poor sensitivity of Lewis coordinated py to sites heterogeneity is quite frequent in the case of oxidic systems, in which all cations possess the same type of coordination (7-fold coordination in the case of monoclinic ZrO_2).

The use of another probe molecule was thus resorted to, namely the ambient temperature adsorption of CO. In fact, in a previous work (*17*), CO uptake at 300 K was able to reveal that, at the surface of activated monoclinic ZrO_2 (ZRP T_2), there are at least two families of Lewis acidic sites, ascribable to coordinatively unsaturated Zr^{4+} centres located respectively in crystallographically defective configurations and on regular patches of some low-index crystal planes.

Figure 7 reports the IR spectra of (100 Torr) CO adsorbed on the reference systems ZRP 673 and ZRP 973 (see the top left and bottom right dotted curves), and on some $ZRS_{473}[n]T_2$ samples. It can be noted that:

(i) At the surface of ZRS_{473}[n]673 samples (shown in the left section of Fig. 7), the Lewis activity towards CO is decreased by the presence of surface sulfates, but not extinguished. As expected, CO uptake is lower the higher the sulfate loading (see curves 1–3), and this confirms that the sulfate groups are bonded to surface Zr ions through Zr–O–S bridges, and indicates that the Zr–O–S linkages are more stable towards vacuum thermal treatments at $T \leq 673$ K than the regular surface hydrated layer of ZrO_2 (*17*).

(ii) The complex absorption due to CO adsorbed onto ZRS_{473}[n]673 samples is shifted towards higher wavenumbers of some 10 cm^{-1} in respect of ZRP 673 (e.g., compare curves 1–3 of Fig. 7 with the top-left dotted curve therein). This indicates that the Lewis surface acidity of the oxide is enhanced by sulfate addition: strong inductive effects are produced by the charge-withdrawing surface sulfate groups, and affect the nearby surface Zr^{4+} ions, so that the σ-charge release from the 5σ lone-pair orbital of CO to the Lewis adsorbing sites is stronger on s.d.-ZrO_2 than on "clean" ZrO_2. These effects have been observed also on other oxidic systems (*18, 19*).

(iii) The absorption due to CO adsorbed onto ZRS 673 samples is complex, and (at least) three components are needed to band-resolve it (see, for instance, the broken-line curves 1 and 3 in Fig. 7). There is a weak and rather well resolved component located at the highest wavenumber ($\nu_{CO} \approx 2205$ cm^{-1}), which is thought to represent CO adsorption onto the few residual Lewis acidic sites located in crystallographically defective configurations; the corresponding CO band absorbs strongly at $\approx$2190 cm^{-1} on ZRP 673, and a $\Delta\nu_{CO}$ of $\approx$15 cm^{-1} indicates that the acidity enhancement brought about by sulfation on this CO species is quite strong. The other two CO components ($\nu_{CO} \approx 2193$ and 2185 cm^{-1} respectively) are thought to represent CO uptake onto regular patches of some low-index crystal planes. The $\Delta\nu_{CO}$ is smaller ($\approx$10 cm^{-1}) in the case of the $\approx$2193 cm^{-1} species than in the case of the $\approx$2205 cm^{-1} one, and indicates an appreciable but smaller acidity enhancement by sulfation, whereas the $\approx$2185 cm^{-1} band is thought not to have a corresponding band on the sulfate-free system, and to be due to sites that have become active towards CO at ambient temperature only as a consequence of the inductive effects from surface sulfates.

The assignment proposed for the CO bands is confirmed by the fact that the intensity of the high $\tilde{\nu}$ CO component does not change appreciably on an increase in the sulfate loading (and, in fact, sulfates on defects were shown to form first and not to increase further at higher S-loadings), whereas the intensity of the two CO compo-

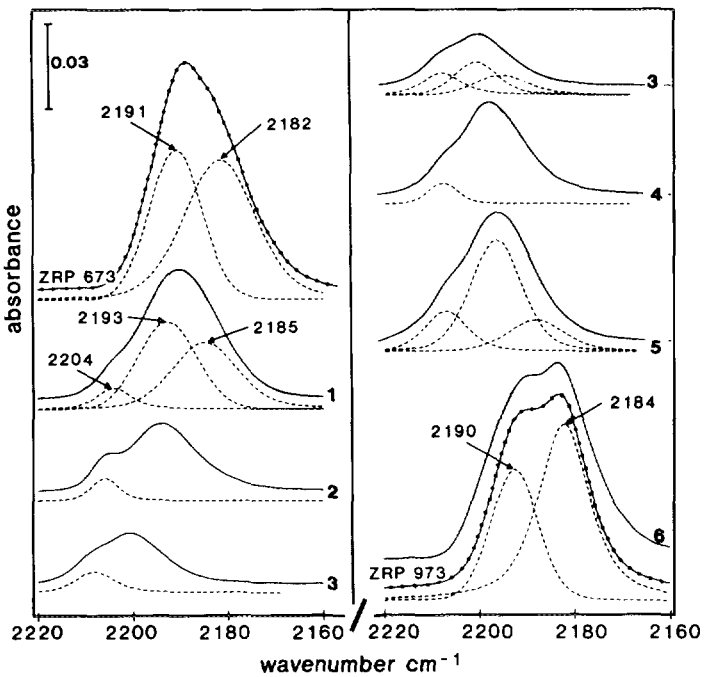

FIG. 7. Absorbance IR spectra of 100 Torr CO adsorbed at 300 K. Dotted lines: the reference pure ZrO_2 samples ZRP 673 (*top left spectrum*) and ZRP 973 (*bottom right spectrum*). Solid lines: the s.d.-ZrO_2 samples ZRS[0.65]673 (1), ZRS[1.3]673 (2), ZRS[2.6]673 (3), ZRS[2.6]773 (4), ZRS[2.6]823 (5), ZRS[2.6]973 (6). Broken lines: computer band-resolved CO components.

nents absorbing at lower $\tilde{\nu}$ keeps decreasing with increasing sulfate loading, i.e., when the sulfate layer is building up on the less energetic regular crystallographic configurations.

More details on the complex CO/ZRS system are not pertinent here, and will be reported elsewhere; for the present work it is sufficient to note that CO uptake at ambient temperature can reveal a wide heterogeneity among the Lewis acidic sites at the surface of s.d.-ZrO_2 from (Zr-ip), and that this heterogeneity could not be revealed by the adsorption of py in the [py-L] form.

(iv) When a s.d.-ZrO_2 from (Zr-ip) is activated at $T \geq 773$ K (see curves 4–6 in Fig. 7), sulfates start decomposing and the absorption of CO adsorbable at 300 K becomes progressively stronger, as expected, and progressively more complex. In particular, the spectra of curves 4 and 5 of Fig. 7 indicate that the situation of the Lewis surface acidity probed by CO uptake during the first stages of the stepwise thermal decomposition of sulfates is quite similar to, but not coincident with the situation probed during the stepwise building up of the sulfate layer (curves 1–3 of Fig. 7): in fact, the temperatures at which the sulfates decompose *in vacuo* are higher than the temperatures at which the sulfate-loaded samples of curves 1–3 were vacuum activated.

When, for activation at ≈973 K, all sulfates are decomposed, the absorption due to adsorbed CO (curve 6 of Fig. 7) again becomes located at the two (lower) wavenumbers typical of CO on nonsulfated ZrO_2, and is virtually indistinguishable from the absorption of CO on ZRP 973 (see the bottom dotted curve of Fig. 7). This indicates that the whole cycle of sulfate formation/sulfate decomposition did not yield an ulti-

mate surface situation appreciably different from that obtainable by direct vacuum activation of ZrO_2 at the same temperature. This datum is also consistent with the minimal alteration of particle size and morphology produced by the sulfation process on the s.d.-ZrO_2 catalysts from (Zr-ip).

CONCLUSIONS

A first remarkable conclusion is that the overall behaviour of s.d.-ZrO_2 systems is quite complex, and depends much more than one would expect (and much more than was already reported by other researchers) on the preparative route adopted. In particular, the behaviour turns out to depend on the nature and characteristics of the precursor material on which the loading step with sulfates is carried out. In fact, the crystallisation trend and the evolution of particle size and morphology with firing/activation temperature of s.d.-ZrO_2 systems from (Zr-ip) are quite different from those reported in the literature for other preparations. Nonetheless, important elements common to all s.d.-ZrO_2 preparations examined so far do exist: for instance, the maximum total acidity is always obtained with specimens that, starting from amorphous, became crystalline. This turns out to be so no matter whether the crystal phase is monoclinic (as in the case of the present samples from (Zr-ip)) or tetragonal (as in the case, for instance, of Arata's ZrO_2–I samples from $ZrOCl_2$ activated at 923 K(9)).

The nature and strength of acidic centres at the surface of the s.d.-ZrO_2 catalysts from (Zr-ip) depend primarily on the type of sulfates present at the surface, and the type of sulfates is found to depend on several preparative parameters. Among them, most important are the overall surface concentration of sulfates, the temperature of (vacuum) activation reached by the sulfated system, and the temperature of ZrO_2 activation prior to sulfate loading. (For comparison, it is noteworthy that loading crystalline ZrO_2 from Zr chloride and/or nitrate with sulfates was found to be detrimental for the catalyst acidity, although no explanation was given, at least in terms of the type of sulfates formed.)

From a structural and morphological point of view, surface sulfation with diluted H_2SO_4 turns out to affect the starting ZrO_2 system less and less, the higher is its crystalline order. In fact, amorphous hydrated ZrO_2 from (Zr-ip) crystallizes upon sulfation, and tiny platelets of the monoclinic phase are stabilized already at ambient temperature (i.e., the usual tetragonal microcrystalline step is skipped entirely), whereas few structural changes (if any) are produced upon sulfation of the microcrystalline monoclinic–tetragonal ZrO_2 mixed systems obtained by firing at $T \geq 683$ K pure ZrO_2 from (Zr-ip).

For any given surface sulfate loading (still far below the full monolayer), the particle morphology of the starting ZrO_2 system turns out to be of primary importance in determining the type and amount of sulfates which form and, consequently, the type and amount of the surface acidity that is induced by surface sulfates. In particular, crystallographically defective terminations (energetically richer and typical of high area unsintered systems) yield the (thermally) most stable sulfate groups. The latter, at least as long as they remain in the form of isolated $(SO_4)^{2-}$ groups, do not induce any Brønsted acidity on the hydrated ZRS system, and on the dehydrated ZRS system induce only very strong Lewis acidic centres. These very strong Lewis sites are shown by CO uptake to be quite scarce, as most of the defective configurations are more favourably occupied by the sulfates.

With increasing surface sulfation, more and more surface Zr^{4+} cations located on regular patches of low-index crystal planes, which in the case of hydrated "clean" ZrO_2 are covered by OH groups, become shielded by sulfate groups. The latter are thermally more stable *in vacuo* than the surface OH groups of regular "clean" ZrO_2 they substituted so that, upon vacuum activation at $T \leq 773$ K, fewer and fewer Lewis acidic sites

can be produced. But the few Lewis acidic sites that are still produced are induced, through inductive effects from nearby sulfates, an acidity unusually high for ZrO_2.

Most sulfate groups which form on the exposed patches of regular crystal planes can induce a protonic (Brønsted) acidic activity, especially if they are in the form of the complex (polynuclear) sulfates favoured by high S loadings. The amount of protonic (Brønsted) acidic sites that these sulfates can induce is strictly determined by the overall surface hydration degree.

The sulfates responsible for the Brønsted acidity of s.d.-ZrO_2 systems represent the most labile fraction of the overall sulfates layer, and no Brønsted acidity is left on sulfated systems from (Zr-ip) that experienced thermal treatment(s) at $T \geq 873$ K.

Among the Lewis acidic centres of s.d.-ZrO_2, those whose acidity is induced by the (thermally) less stable sulfates located on portions of low-index crystal planes belong to (at least) two energetically slightly different families (as shown by CO uptake), and are converted upon surface hydration into two families of Brønsted centres (as shown by py uptake).

ACKNOWLEDGMENTS

This research was partly financed with funds of the CNR (Rome), Progetto Finalizzato Materiali Speciali. The authors gratefully acknowledge the contributions of Dr. M. Baricco (University of Turin) in obtaining and interpreting the XRD data, and Prof. C. Sarzanini (University of Turin) in carrying out the analysis of sulfates.

REFERENCES

1. Hino, H., and Arata, K., *J. Chem. Soc. Chem. Commun.*, 851 (1980).
2. Kayo, A., Yamaguchi, T., and Tanabe, K., *J. Catal.* **83,** 99 (1983).
3. Nitta, M., Sakoh, H., and Aomura, K., *Appl. Catal.* **10,** 215 (1984).
4. Tanabe, K., *Mater. Chem. Phys.* **13,** 347 (1985).
5. Jin, T., Yamaguchi, T., and Tanabe, K., *J. Phys. Chem.* **90,** 4794 (1986).
6. Bensitel, M., Saur, O., Lavalley, J. C., and Mabilon, G. *Mater. Chem. Phys.* **17,** 249 (1987).
7. Komarov, V. S., and Sinilo, M. F., *Kinet. Katal.* **29,** 605 (1988).
8. Nascimento, P., Akratopoulou, C., Oszagyan, M., Coudurier, G., Travers, C., Joly, J. F., and Vedrine, J. C., in "Proceedings, 10th International Congress on Catalysis, Budapest, 1992," Paper O 80.
9. Arata, K., *Adv. Catal.* **37,** 165 (1990).
10. Umansky, B., Engelhardt, J., and Hall, W. K., *J. Catal.* **127,** 128 (1991).
11. Morterra, C., Orio, L., Bolis, V., and Ugliengo, P., *Mater. Chem. Phys.* **29,** 457 (1991).
12. Bensitel, M., Saur, O., Lavalley, J. C., and Morrow, B. A., *Mater. Chem. Phys.* **19,** 147 (1988).
13. Nakamoto, K., "Infrared and Raman Spectra of Inorganic and Coordination Compounds," p. 249, Wiley–Interscience, New York, 1986.
14. Colthup, N. B., Daly, L. H., and Wiberley, S. E., "Introduction to Infrared and Raman Spectroscopy," p. 353, Academic Press, New York, 1975.
15. Parry, E. P., *J. Catal.* **2,** 371 (1963).
16. Morterra, C., Cerrato, G., Visca, M., and Lenti, D. M., *Chem. Mater.* **3,** 132 (1991).
17. Morterra, M., Orio, L., and Emanuel, C., *J. Chem. Soc. Faraday Trans.* **86,** 3003 (1990).
18. Garrone, E., Bolis, V., Fubini B., and Morterra, C., *Langmuir* **5,** 892 (1989).
19. Bolis, V., Fubini, B., Garrone, E., Morterra, C., and Ugliengo, P., *J. Chem. Soc. Faraday Trans.* **88,** 391 (1992).